

**A HEURISTIC REMARK  
ON THE PERIODIC VARIATION  
IN THE NUMBER OF SOLAR NEUTRINOS  
DETECTED ON EARTH**

H.J. Haubold

UN Outer Space Office, Vienna International Centre, Vienna, Austria

and

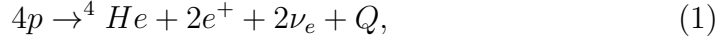
A.M. Mathai

Department of Mathematics and Statistics, McGill University, Montreal,  
Canada

Abstract. Four operating neutrino observatories confirm the long standing discrepancy between detected and predicted solar neutrino flux. Among these four experiments the Homestake experiment is taking data for almost 25 years. The reliability of the radiochemical method for detecting solar neutrinos has been tested recently by the GALLEX experiment. All efforts to solve the solar neutrino problem by improving solar, nuclear, and neutrino physics have failed so far. This may also mean that the average solar neutrino flux extracted from the four experiments may not be the proper quantity to explain the production of neutrinos in the deep interior of the Sun. Occasionally it has been emphasized that the solar neutrino flux may vary over time. In this paper we do address relations among specific neutrino fluxes produced in the proton-proton chain that are imposed by the coupled systems of non-linear partial differential equations of solar structure and kinetic equations by focusing our attention on a statistical interpretation of selected kinetic equation of PPII/PPIII branch reactions of the proton-proton chain. A fresh look at the statistical implications for the outcome of kinetic equations for nuclear reactions may shed light on recent claims that the  ${}^7\text{Be}$ -neutrino flux of the Sun is suppressed in comparison to the pp- and  ${}^8\text{B}$  neutrino fluxes and may hint at that the solar neutrino flux is indeed varying over time as shown by the Homestake experiment.

# 1 Solar Nuclear Energy Generation: Proton-Proton-Chain

The nuclear energy source in the Sun is believed to be the proton-proton chain, in which four protons fuse to form one  ${}^4\text{He}$  nucleus, i.e.



where  $Q = M({}^4\text{He}) - 4M_p - 2M_e \approx 26.73\text{MeV}$  denotes the energy release. The three different branches (PPI, PPII, PPIII) to accomplish the formation of  ${}^4\text{He}$  in the pp-chain are shown in Figure 1. Neutrinos are produced in the pp-chain by nuclear fusion reactions, beta-decay, and electron capture. The dominant reactions (PPI, 86% of the produced  ${}^4\text{He}$ ) produce the great majority of low energy solar neutrinos ( $\Phi_\nu^{SSM}(pp) \approx 6.0 \times 10^{10} \nu\text{cm}^{-2}\text{s}^{-1}$ ,  $\Phi_\nu^{SSM}(pp) \sim T_c^{-1.2}$ , where  $T_c$  denotes the temperature at the centre of the Sun) and their number should be a firm prediction of any solar model because it is closely tied to the solar luminosity. The second branch of the pp-chain (PPII, 14% of the produced  ${}^4\text{He}$ ) yields the  ${}^7\text{Be}$  neutrinos at two discrete energies ( $\Phi_\nu^{SSM}({}^7\text{Be}) \approx 4.9 \times 10^9 \nu\text{cm}^{-2}\text{s}^{-1}$ ,  $\Phi_\nu^{SSM}({}^7\text{Be}) \sim T_c^8$ ). In the third branch of the pp-chain, the very rare case (PPIII, 0.02% of the produced  ${}^4\text{He}$ ), radioactive  ${}^8\text{B}$  is produced which decays ultimately and is the source of high energy  ${}^8\text{B}$  neutrinos ( $\Phi_\nu^{SSM}({}^8\text{B}) \approx 5.5 \times 10^6 \nu\text{cm}^{-2}\text{s}^{-1}$ ,  $\Phi_\nu^{SSM}({}^8\text{B}) \sim T_c^{18}$ ). The specific neutrino fluxes are taken from the Standard Solar Model (SSM) of Bahcall and Pinsonneault (1992). The overall energy production of the pp-chain is  $Q = 26.73\text{MeV}$ , however, the three branches produce a different amount of energy (PPI:  $E_\gamma = (26.73 - 0.265)\text{MeV}$ , PPII:  $E_\gamma = (26.73 - 0.861)\text{MeV}$ , PPIII:  $E_\gamma = (26.73 - 7)\text{MeV}$ ) due to the energy loss carried off by elusive neutrinos. The fluxes of high energy solar neutrinos are especially sensitive to the central temperature,  $T_c$ , mainly because of the energy dependence of the cross sections of the respective nuclear reactions. The branching ratios (the percentage of which each branch of the pp-chain contributes to the production of  ${}^4\text{He}$ ) are strongly dependent on the nuclear reaction probabilities and on the density and temperature profiles inside the Sun. Assuming that the Sun is in a state of quasistatic equilibrium, the solar luminosity  $L_\odot$  tells us the total energy generation rate which can be turned into a constraint on the total solar neutrino fluxes, that is

$$L_\odot = 13.1(\phi_\nu(pp) - \phi_\nu({}^7\text{Be}) - \phi_\nu({}^8\text{B})) + 25.6\phi_\nu({}^7\text{Be}) + 19.5\phi_\nu({}^8\text{B}). \quad (2)$$

The luminosity  $L_{\odot}$  observed at the current stage of evolution of the Sun corresponds to the energy that was generated in the gravitationally stabilized solar fusion reactor  $10^7$  yr ago (Helmholtz-Kelvin timescale). The quasistatic assumption allows one to equate the present luminosity with the present nuclear energy production rate (Mathai and Haubold, 1988). Normalizing the neutrino fluxes in (2) to those of the Standard Solar Model ( $\Phi_{\nu} = \phi_{\nu}/\phi_{\nu}^{SSM}$ ) leads to a luminosity constraint indicating the degree of contribution of the respective neutrino flux to the total solar neutrino emission:

$$1 = 0.913\Phi_{\nu}(pp) + 0.071\Phi_{\nu}({}^7Be) + 0.00004\Phi_{\nu}({}^8B). \quad (3)$$

To reveal how the pp-chain operates in the Sun is to measure the individual neutrino fluxes  $\phi_{\nu}(pp)$ ,  $\phi_{\nu}({}^7Be)$ , and  $\phi_{\nu}({}^8B)$  in (3), thereby fixing the branching ratios of PPI, PPII, and PPIII as indicated in Figure 1. Four experiments are in operation now to accomplish this solar neutrino spectroscopy. Kamiokande measures exclusively the high-energy flux  $\phi_{\nu}({}^8B)$ , thus PPIII, in real-time spectroscopy. Homestake observes primarily  $\phi_{\nu}({}^8B)$  and to a much lesser extent  $\phi_{\nu}({}^7Be)$ , that is, the branching of PPII and PPIII. GransSasso/Baksan detects primarily the low-energy flux  $\phi_{\nu}(pp)$  and to a lesser extent the fluxes  $\phi({}^7Be)$  and  $\phi_{\nu}({}^8B)$ , thus focusing on the branching of PPI and PPII/PPIII.

## 2 Spatial Distribution of Solar Neutrino Sources: Standard Solar Model

Figure 2 shows the neutrino production as a function of the dimensionless distance variable  $x = R/R_{\odot}$ , starting from the center of the Sun for the Standard Solar Model (Bahcall and Pinsonneault, 1992). We note that experiments for the detection of solar neutrinos are looking into different depths of the solar core as they are only sensitive to specific neutrinos produced in the respective nuclear reactions. The region in which the low-energy pp-neutrino flux is produced is very similar to that of the total nuclear energy generation. Because of its strong temperature dependence, the high-energy  ${}^8B$ -neutrino production is peaked at the very small radius  $x = 0.05$  and is generated in a much narrower region in comparison to the other two neutrino sources (Table 3).

The contribution of the neutrino fluxes  $\phi_\nu(pp)$ ,  $\phi_\nu(^7Be)$ , and  $\phi_\nu(^8B)$  to the Homestake, Kamiokande, and GranSasso/Baksan experiments is

$$\phi_\nu(\text{Homestake}) \approx 6.2\phi_\nu(^8B) + 1.2\phi_\nu(^7Be)SNU, \quad (4)$$

$$\phi_\nu(\text{Kamiokande}) = \phi_\nu(^8B)\Phi_\nu(^8B), \quad (5)$$

$$\phi_\nu(\text{GranSasso/Baksan}) \approx 13.8\phi_\nu(^8B) + 35.8\phi_\nu(^7Be) + 70.8\phi_\nu(pp). \quad (6)$$

The coefficients in Equation (4)-(6) are corresponding to the capture rates predicted by the Standard Solar Model for each respective solar neutrino source.

Table 1 summarizes the predictions of the total capture rates of the Standard Solar Model for the Kamiokande, Homestake, and GranSasso/Baksan experiments. The Kamiokande solar neutrino flux is given in units of  $10^6\nu\text{cm}^{-2}\text{s}^{-1}$ , while the Homestake and GranSasso/Baksan rates are given in solar neutrino units ( $1SNU \equiv 10^{-36}\nu\text{atom}^{-1}\text{s}^{-1}$ ). The uncertainties shown in Table 1 are  $1\sigma$ .

Experiment	Kamiokande	Homestake	GranSasso/Baksan
Predicted capture rate	$5.69 \pm 0.82$	$8.0 \pm 3.0$	$131.5 \pm_{17}^{21}$

Table 1.

### 3 Four Solar Neutrino Experiments: Solar Neutrino Problem and $^7\text{Be}$ -Neutrino Deficiency

Experiment	Reaction	Energy threshold	Location
Kamiokande	$\nu_e + e^- \rightarrow \nu_e + e^-$	$7.5\text{MeV}$	Japan
Homestake	$\nu_e + ^{37}\text{Cl} \rightarrow ^{37}\text{Ar} + e^-$	$0.814\text{MeV}$	USA
GranSasso (GALLEX)	$\nu_e + ^{71}\text{Ga} \rightarrow ^{71}\text{Ga} + e^-$	$0.233\text{MeV}$	Italy
Baksan (SAGE)	$\nu_e + ^{71}\text{Ga} \rightarrow ^{71}\text{Ge} + e^-$	$0.233\text{MeV}$	Russia

Table 2.

There are four experiments currently operating to detect neutrinos coming from the Sun (Table 2). The Kamiokande experiment is a water Čerenkov detector which measures the energy of the scattered electrons (Nakamura, 1993). Due to its energy threshold it is only sensitive to the high-energy  ${}^8B$  neutrinos from branch PPIII of the pp-chain. The Homestake experiment consists of  $10^5$  gallons of  $C_2Cl_4$  and detects solar neutrinos via capture on the chlorine (Davis, 1993). Its energy threshold allows to detect the higher energy line of  ${}^7Be$ -neutrinos from branch PPII as well as the high-energy  ${}^8B$  neutrinos from branch PPIII. The two gallium experiments at GranSasso and Baksan are sensitive to the low energy pp-neutrinos from the PPI branch of the pp-chain as well as to the higher energy  ${}^7Be$ - and  ${}^8B$ -neutrinos (Anselmann et al., 1994; Abdurashitov et al., 1994). The predicted contributions to the Homestake and GranSasso/Baksan experiments based on the Standard Solar Model are shown in Table 3.

Neutrino source	Homestake experiment	Percentage of total capture rate	GranSasso/Baksan experiments
pp	0.0	≡ 0%	70.8
pep	0.2	≡ 2.5%	3.1
${}^7Be$	1.2	≡ 15%	35.8
${}^8B$	6.2	≡ 77.5%	13.8
${}^{13}N$	0.1	≡ 1.25%	3.0
${}^{15}O$	0.3	≡ 3.75%	4.9
total capture rate	$8.0 \pm 3.0$	≡ 100%	$131.5 \pm_{17}^{21}$

Table 3.

The experimental results of the four solar neutrino experiments are given in Table 4 and can be compared with the predictions of the Standard Solar Model as shown in Table 1.

Experiment	Detected capture rate	Detected capture rate/ predicted capture rate
Kamiokande	$2.89_{-0.21}^{+0.22} \pm 0.35$	$0.50 \pm 0.07$
Homestake	$2.55 \pm 0.17 \pm 0.18$	$0.32 \pm 0.03$
GranSasso/ Baksan	$77 \pm 9$	$0.59 \pm 0.07$

Table 4.

From Table 4 it is evident that the results of the four experiments are between  $1/3$  and  $1/2$  of the neutrino capture rates predicted by the Standard Solar Model. This deficit of solar neutrinos is called the solar neutrino problem which poses a serious conflict with the constraint of the overall solar luminosity in (2) and (3). Additionally, the comparison of the three detected capture rates in Table 4 with the predicted capture rates in Tables 1 and 3 shows that the Kamiokande rate is less suppressed than the Homestake rate. Because the Homestake experiment has a lower energy threshold, the lower detected capture rate suggests that the  ${}^7\text{Be}$ -neutrinos are more suppressed than the high energy  ${}^8\text{B}$ -neutrinos. However, any reduction of the  ${}^7\text{Be}$  production rate by lowering the temperature  $T_c$  would affect immediately both the  ${}^7\text{Be}$  and  ${}^8\text{B}$  neutrino production equally. This fact seems to pose an additional problem in finding a solution of the solar neutrino problem in terms of solar, nuclear, and neutrino physics on which the Standard Solar Model is based. This is particularly true for the so-called cooler Sun models (Castellani et al., 1994).

## 4 Argon-Production Rate of the Homestake Experiment: Variations Over Time

Figure 3 shows the  ${}^{37}\text{Ar}$  production rate detected by the Homestake experiment from 1970.8 to 1991.6 (Davis, 1993). The average  ${}^{37}\text{Ar}$  production rate (combined likelihood function) for the 94 individual runs shown was  $0.509 \pm 0.031$  argon atoms per day. Subtracting a total background  ${}^{37}\text{Ar}$  production rate of  $0.08 \pm 0.03$  atoms per day yields the production rate that can be ascribed to solar neutrinos:  $0.429 \pm 0.043$  atoms per day or  $2.28 \pm 0.23$  SNU (the rate in SNU is equal to 5.31 times the captures per day in the Homestake experiment). This average capture rate is commonly compared to the

predictions of the Standard Solar Model as shown in Tables 1 and 3 for the pp-chain and the CNO cycle. This procedure does not take into account in any way the apparent time variation in the observed  $^{37}\text{Ar}$  production rate evident in Figure 3.

Figure 4 shows a five-point moving average of the  $^{37}\text{Ar}$  production rate, removing high frequency noise from the actual time series collected in the Homestake experiment as shown in Figure 3. One notes in the five-point moving average that in the periods 1978 to 1979 and 1987 to 1988 a suppression of the  $^{37}\text{Ar}$  production rate seems to occur. The overall shape of the five-point moving average suggests that there are two distinctive epochs spanning the time periods 1971 to 1980 and 1980 to 1989. Each epoch shows a shock-like rise and subsequent rapid decline of the  $^{37}\text{Ar}$  production rate. Further, the five-point moving average of the  $^{37}\text{Ar}$  production rate reveals that each of the two distinct cycles covers a time period of around 9 years. Each cycle exhibits a slow but shock-like increase, reaching a peak, succeeded by a rapid decrease to a minimum value of the  $^{37}\text{Ar}$  production rate. This pattern is repeated for a second nine-year period and seems to start for a third period in 1989 (Haubold and Mathai, 1994). Each of these cycles can be reproduced by a mechanism discussed in the following Section. Fourier analysis of the  $^{37}\text{Ar}$  production rate data in Figure 3 reveals a power spectrum showing the harmonic content in this time series in terms of a series of distinctive periodicities which is shown in Figure 5. Fourier analysis also indicates that the harmonic content in the  $^{37}\text{Ar}$  production rate data is dominated by periodicities of 0.57, 2.2, 4.8, and 8.3 years (Haubold and Gerth, 1990).

## 5 Kinetic Equations: Lifetime Densities

The production and destruction of nuclei in the proton-proton chain of reactions can be described by kinetic equations governing the change of the number density  $N_i$  of species  $i$  over time, that is,

$$\frac{d}{dt}N_i = - \sum_j N_i N_j \langle \sigma v \rangle_{ij} + \sum_{k,l \neq i} N_k N_l \langle \sigma v \rangle_{kl}, \quad (7)$$

where  $\langle \sigma v \rangle_{mn}$  denotes the reaction probability for an interaction involving species  $m$  and  $n$ , and the summation is taken over all reactions which either

produce or destroy the species  $i$ . The first sum in (7) can also be written as

$$-\sum_j N_i N_j \langle \sigma v \rangle_{ij} = -N_i \left( \sum_j N_j \langle \sigma v \rangle_{ij} \right) = -N_i a_i, \quad (8)$$

where  $a_i$  is the statistical expected number of reactions per unit volume per unit time destroying the species  $i$ . The reciprocal of the quantity  $a_i$  is the lifetime of species  $i$  for interaction with species  $j$  for all  $j$ . It is also a measure of the speed in which the reaction proceeds. If the reaction results in the production of a neutrino, for example, then the reciprocal of  $a_i$  is the expected time it takes to produce this neutrino in the solar interior. In the following we are assuming that there are  $N_j$  ( $j = 1, \dots, i, \dots$ ) of species  $j$  per unit volume and that for a fixed  $N_i$  the numbers of other reacting species that react with the  $i$ -th species are constants in a unit volume. Following the same argument we have for the second sum in (7) accordingly,

$$+\sum_{k,l \neq i} N_k N_l \langle \sigma v \rangle_{kl} = +N_i b_i,$$

where  $N_i b_i$  is the statistical expected number of the  $i$ -th species produced per unit volume per unit time for a fixed  $N_i$ . Note that by nature the number density of species  $i$ ,  $N_i = N_i(t)$ , is a function of time while the  $\langle \sigma v \rangle_{mn}$  are supposed to depend only on the temperature but not on the time  $t$  and number densities  $N_j$ . Then equation (7) implies that

$$\frac{d}{dt} N_i(t) = -(a_i - b_i) N_i(t). \quad (9)$$

For equation (9) we have three cases,  $c_i = a_i - b_i > 0$ ,  $c_i < 0$ ,  $c_i = 0$ , of which the last case says that  $N_i(t)$  does not vary over time, which means that the forward and reverse reactions involving species  $i$  are in equilibrium. The first two cases exhibit that either the destruction ( $c_i > 0$ ) of species  $i$  or production ( $c_i < 0$ ) of species  $i$  dominates.

For the case  $c_i > 0$  we have

$$\frac{d}{dt} N_i(t) = -c_i N_i(t),$$

and it follows that

$$N_i(t) dt = N_i(0) e^{-c_i t} dt, \quad (10)$$

where  $N_i(0)$  is the number density of species  $i$  at time  $t = 0$ . If  $c_i$  in (10) is a function of time, say  $c_i(t)$ , then  $c_i t$  in (10) is to be replaced by  $\int dt c_i(t)$ . If the arrival distributions for the other species are Poisson, then  $c_i(t)$  will be of the form  $d_i t$ , where  $d_i > 0$  independent of  $t$ . In this case the exponent in (10) is  $\int dt c_i(t) = d_i t^2/2$ . Contrarily, when  $c_i$  is a constant, the total number of reactions in the time interval  $0 \leq t \leq t_0$  is given by

$$\int_0^{t_0} dt N_i(t) = N_i(0) \int_0^{t_0} dt e^{-c_i t} = \frac{N_i(0)}{c_i} (1 - e^{-c_i t_0}). \quad (11)$$

In (11),  $1 - e^{-c_i t_0}$  is the probability that the lifetime of species  $i$  is  $\leq t_0$  when  $t$  has the density

$$f(t) = c_i e^{-c_i t}, 0 \leq t \leq \infty, c_i > 0, \quad (12)$$

or

$$N_i(t) = \frac{N_i(0)}{c_i} f(t). \quad (13)$$

When  $c_i = c_i(t) = d_i t$  then

$$N_i(t) = \left( \frac{\pi}{2d_i} \right)^{1/2} N_i(0) h(t), \quad (14)$$

where

$$h(t) = \left( \frac{2d_i}{\pi} \right)^{1/2} e^{-d_i t^2/2}, 0 \leq t \leq \infty, d_i > 0. \quad (15)$$

The density in (12) will be called the lifetime density for the destruction of species  $i$ , with the expected mean lifetime

$$E(t) = \frac{1}{c_i}. \quad (16)$$

If the lifetime density is as given in (15) then

$$E(t) = \left( \frac{2}{\pi d_i} \right)^{1/2}. \quad (17)$$

From (12) and (16) we can make the following observations:

(i)  $c_i$  can be interpreted as a measure of net destruction, the larger the value of  $c_i$  the faster the net destruction.

(ii)  $\frac{N_i(0)}{c_i} f(t) \Delta t$  can be interpreted as the amount of net destruction over the small interval of time  $\Delta t$ . The faster the net destruction the shorter the lifetime.

(iii) The quantity

$$\int_0^\infty dt \frac{N_i(0)}{c_i} f(t) = \frac{N_i(0)}{c_i} \quad (18)$$

can be interpreted as the total net destruction of species  $i$  starting with the initial number  $N_i(0)$ .

(iv) If the net destruction of species  $i$  produces a species  $k$ , for example a neutrino, then the number produced is proportional to  $\frac{N_i(0)}{c_i}$ .

If the lifetime for the production of a species  $k$  due to the net destruction of species  $i$  is denoted by  $\tau$ , then  $\tau$  is a constant multiple of  $t$ , say  $\tau = \alpha_1 t$ , where  $t$  has the lifetime density  $f(t)$ . But the densities of  $t$  and  $\alpha_1 t$  ( $\alpha_1 > 0$ ) belong to the same family of distributions and hence the density of  $\tau$  can be written as

$$f(\tau) = \theta_i e^{-\theta_i \tau}, \theta_i > 0, \tau > 0, \quad (19)$$

where  $\theta_i = c_i/\alpha_1$  and thus the total production is  $\alpha_1 \frac{N_i(0)}{c_i}$ .

## 6 Dampening of Reactions: Poisson Arrivals

Suppose that after a certain period of time of net destruction, say  $t_0$ , a dampening effect starts to slow down the net destruction of species  $i$  with initial number  $N_i(0)$ . Let this dampening variable be denoted by  $\tau_2$ , where  $\tau_2$  is again proportional to the lifetime, say  $\alpha_2 t$ . Then the lifetime density associated with  $\tau_2$  is of the exponential type, belonging to the same family as in (19). Let  $\tau_1$  and  $\tau_2$  be independently acting or statistically independent. Let the delay in time for  $\tau_2$  to start be  $c = \alpha_2 t_0$  and let the densities of  $\tau_1$  and  $\tau_2$  be denoted by

$$f_j(\tau_j) = \beta_j e^{-\beta_j \tau_j}, \tau_j > 0, \beta_j > 0, j = 1, 2 \quad (20)$$

where  $\beta_1 = \theta_i = c_i/\alpha_1$  of (19) and let  $\beta_2 = c_i/\alpha_2$ . Then the net destruction of species  $i$  is proportional to  $u = \tau_1 - (\tau_2 - c) = \tau_1 - \tau_2 + c$  with the joint density of  $\tau_1$  and  $\tau_2$  given by

$$f(\tau_1, \tau_2) = \beta_1 \beta_2 e^{-(\beta_1 \tau_1 + \beta_2 \tau_2)}, \tau_j > 0, \beta_j > 0, j = 1, 2 \quad (21)$$

due to the statistical independence of  $\tau_1$  and  $\tau_2$ . The density of  $u$ , denoted by  $g(u)$ , is the following (Mathai, 1993)

$$g(u) = \begin{cases} \frac{\beta_1\beta_2}{\beta_1+\beta_2} e^{-\beta_1(u-c)}, & c \leq u < \infty \\ \frac{\beta_1\beta_2}{\beta_1+\beta_2} e^{\beta_2(u-c)}, & -\infty < u \leq c \end{cases} \quad (22)$$

where

$$\frac{\beta_1\beta_2}{\beta_1 + \beta_2} = \frac{c_i}{\alpha_1 + \alpha_2},$$

observing that  $\beta_1 = c_i/\alpha_1$  and  $\beta_2 = c_i/\alpha_2$ . If the net destruction of species  $i$  is exceeding the dampening rate, then  $\beta_1 > \beta_2$  and the following Figure 6 illustrates the behaviour of the density  $u$  in (22).

Figure 6 shows a non-symmetric Laplacian, slowly rising and rapidly falling. At the time  $t = t_0$  the net destruction of species  $i$  is given by  $\frac{N_i(0)}{c_i}(1 - e^{-c_i t_0})$ . Then the production of species, for example neutrinos, as a result of the net destruction of species  $i$ , in an instant of time is given by

$$\alpha_1\alpha_2 \left( \frac{N_i(0)}{c_i} \right)^2 (1 - e^{-c_i t_0}) g(u) du, \quad (23)$$

which is a constant multiple of  $g(u)$ , where  $g(u)$  is given in (22). Hence the shape of the curve for the net destruction of species  $i$  and the resulting production of species  $k$  will be the same as of  $g(u)$  shown in Figure 6. The production of resulting species in a small interval of time  $\Delta t$  is  $A g(u) \Delta t$  with  $t_0 = c/\alpha_2$  starting with a constant initial number  $N_i(0)$  of species  $i$ , where

$$A = \alpha_1\alpha_2 \left( \frac{N_i(0)}{c_i} \right)^2 \left( 1 - e^{-\frac{c_i}{\alpha_2} c} \right), \quad (24)$$

since  $\int_{-\infty}^{+\infty} du g(u) = 1$ . Here the integration is done from  $-\infty$  to  $+\infty$ . Note however, that when  $c$  is large enough the probability for  $u$  being negative will be negligibly small and hence  $A$  in (24) is a good approximation to the total production.

We observe in (24) that when  $c$  is small,  $A$  is small and  $A$  is an increasing function of  $c$  as shown in Figure 7.

Note that  $A$  in (24) is the result of assuming that the initial number  $N_i(0)$  of species  $i$  per unit volume is a constant. If the species  $i$  is arriving

to the unit volume according to a Poisson distribution with parameter  $\lambda_i$  (Poisson arrivals), then  $N_i(0)$  in (24) as well as in the previous formulae is to be replaced by its expected value, that is  $E[N_i(0)] = \lambda_i$  in the considered case. In Poisson arrivals one can take the expected number to be  $\lambda_i = \gamma_i t$ , where  $t$  is the duration of destruction and  $\gamma_i$  is a constant independent of time  $t$ . In this case  $A$  in (24) becomes

$$A = \frac{\alpha_1 \alpha_2}{c_i^2} \gamma_i^2 t^2 (1 - e^{-c_i t_0}), \quad (25)$$

where  $t_0 = c/\alpha_2$  is the time where the dampening effect starts.

## 7 Proton-Proton Chain: Branches II and III

The fusion of four protons to produce one helium nucleus in the pp-chain is accomplished in at least three different branches in the chain (Figure 1). This branching results in uncertainties of the predictions of the  ${}^7\text{Be}$ - and  ${}^8\text{B}$  neutrino fluxes in the Standard Solar Model and needs particular attention in discussing the results of those solar neutrino experiments which are detecting exclusively  ${}^7\text{Be}$ - and  ${}^8\text{B}$  neutrinos (Homestake and Kamiokande experiments in Tables 1,2, and 4). Without any branching in the pp-chain, the number of all reactions and neutrinos would be equal, that means

$$\phi_\nu(pp) = \phi({}^8\text{B}) = N.$$

As shown in Figure 1,  ${}^3\text{He}$  can interact with another  ${}^3\text{He}$  nucleus to produce right away  ${}^4\text{He}$  (PPI branch), or  ${}^3\text{He}$  can fuse with  ${}^4\text{He}$  to produce a  ${}^7\text{Be}$  nucleus and subsequently to open branches II and III of the pp-chain. The branching ratio  $r$  is determined by the reaction probabilities  $\langle \sigma v \rangle_{ij}$  and number densities  $N_i$ :

$$\frac{r}{1-r} = \frac{\langle \sigma v \rangle_{34}}{\langle \sigma v \rangle_{33}} \cdot \frac{N_4}{N_3}, \quad (26)$$

where the notations have been explained in the preceding section. With regard to branches II and III in Figure 1,  ${}^7\text{Be}$  can capture an electron to emit a  ${}^7\text{Be}$  neutrino, or it can fuse with a proton to produce  ${}^8\text{B}$  which immediately decays and produces a  ${}^8\text{B}$  neutrino. The branching ratio  $r'$  for PPII and PPIII is

$$\frac{r'}{1-r'} = \frac{\langle \sigma v \rangle_{17}}{\langle \sigma v \rangle_{e7}} \cdot \frac{N_1}{N_e}. \quad (27)$$

With (26) and (27) the following relations between the number of chains to produce  ${}^4\text{He}$  and the neutrino fluxes produced by the three branches are established,

$$\phi_\nu(pp) = \frac{N}{2}(2 - r), \quad (PPI), \quad (28)$$

$$\phi_\nu({}^7\text{Be}) = \frac{N}{2}r(2 - r'), \quad (PPII), \quad (29)$$

$$\phi_\nu({}^8\text{B}) = \frac{N}{2}rr', \quad (PPIII). \quad (30)$$

Equations (28) to (30) show the link of the three branches of the pp-chain which is eventually governed by the reaction probabilities  $\langle \sigma v \rangle_{ij}$  and number densities  $N_i$  in the system of kinetic equations in (7) and by the profiles of density and temperature of the solar model. Basic assumptions for equations (28) to (30) are that the Sun is in thermal equilibrium which fixes the number of chains through (2) and that the nuclei responsible for neutrino production are in thermal equilibrium with the ambient plasma which allows to determine the neutrino fluxes by the reaction probabilities. For the latter assumption the characteristic time for significant energy exchange by Coulomb collisions between reacting species must be orders of magnitude less than the characteristic time it takes to produce a neutrino in the solar interior (Maxwell-Boltzmann reaction rates). These basic assumptions still leave the question open on what is relevant for branching governed by kinetic equations: The time for reducing the protons to thermal equilibrium with the ambient plasma ( $\approx 10^{-20}\text{yr}$ ) or the lifetime of a proton to undergo a reaction with a second proton to produce, among other species, a neutrino ( $\approx 10^{10}\text{yr}$ )? This question will be addressed in the following section for three reactions of the branches II and III of the pp-chain.

## 8 Production - Dampening Mechanism: Laplacian Behaviour

Consider three sets of Laplacians of the type given in Figure 6, one set consisting of one Laplacian with  $t_0 = \frac{1}{2}(1)$  units of time, five successive Laplacians with  $t_0 = \frac{1}{2}(0.2)$  units of time each in the second set, and the third set consisting of eight successive Laplacians with  $t_0 = \frac{1}{2}(0.125)$  units

of time each. Suppose that we consider the Laplacians for a total arbitrary time interval of  $t = 1$  unit of time. Let the total destruction of species  $i$  by one Laplacian of set 1, the five Laplacians of set 2, and the 8 Laplacians of set 3 be denoted by  $A_1, A_2, A_3$  respectively. Then we have from (25)

$$\begin{aligned} A_1 &= \frac{\alpha_1 \alpha_2}{c_i^2} \gamma_i^2 [1(1)^2] \left(1 - e^{-c_i \frac{1}{2}(1)}\right), \\ A_2 &= \frac{\alpha_1 \alpha_2}{c_i^2} \gamma_i^2 [5(0.2)^2] \left(1 - e^{-c_i \frac{1}{2}(0.2)}\right), \\ A_3 &= \frac{\alpha_1 \alpha_2}{c_i^2} \gamma_i^2 [8(0.125)^2] \left(1 - e^{-c_i \frac{1}{2}(0.125)}\right). \end{aligned} \quad (31)$$

If  $c_i$  is large so that  $e^{-c_i(\cdot)}$  is negligible, then the total contributions coming from the three sets are respectively,

$$\frac{A_j}{A_1 + A_2 + A_3} = 0.755, 0.15, 0.095, j = 1, 2, 3 \quad (32)$$

respectively, that is, 75.5%, 15%, and 9.5% for each of the three reactions.

The Laplacians can be approximated by using triangles in the following way. From Figure 6 it is noted that the maximum height of the Laplacian is at  $u = c$  which will then be

$$\frac{\beta_1 \beta_2}{\beta_1 + \beta_2} = \frac{c_i}{\alpha_1 + \alpha_2}. \quad (33)$$

Suppose that  $\alpha_2 = 3\alpha_1$ , which will imply that  $\beta_1 = \frac{c_i}{\alpha_1}$  and  $\beta_2 = \frac{c_i}{3\alpha_1}$ , which in turn means that the net destruction rate is three times the dampening rate. Suppose that  $\beta_1 = \sqrt{3}b$ , where  $b > 0$  is a constant and  $t_0 = \frac{3}{4}b$ . Then the maximum height of the Laplacian in Figure 6 is

$$\frac{\beta_1 \beta_2}{\beta_1 + \beta_2} = \frac{c_i}{\alpha_1 + \alpha_2} = \frac{\sqrt{3}b}{4}. \quad (34)$$

In this case the Laplacian approximates to the following triangle shown in Figure 8.

If we take three sets of triangles shown in Figure 8, where the first set consists only of one triangle with  $b = 1$  time unit, the second set contains 5 successive triangles with  $b = 0.2$  time units each, and in the third set there are 8 successive triangles with  $b = 0.125$  units each, and if the total areas of these

three sets of triangles are denoted by  $A_1$ ,  $A_2$ , and  $A_3$  similar to (31), then the respective areas are in the proportion 75.5, 15, and 9.5 percent respectively (see Table 5).

Total area	Contribution to the 9 year cycle	$^{37}\text{Ar}$ production rate of the Homestake experiment (Table 3)
1 triangle Reaction 1	75.5 %	$^8\text{B}$ contributes 77.5%
5 triangles Reaction 2	15.0%	$^7\text{Be}$ contributes 15%
8 triangles Reaction 3	9.5%	

Table 5.

Triangles as the ones shown in Figure 8 have been used in the following graph, where in Figure 9,  $\alpha$  and  $\beta$  denote the shifts in the starting point of the set of 5 and of the set of 8 triangles, respectively. The starting point of the one big triangle has been chosen as  $t = 0$ .

## 9 Conclusion

The time variation of the argon production in the Homestake experiment which is ascribed to be produced by solar neutrinos can be explained as follows. The original Homestake data, but more distinctively the five-point moving average of the data, seem to show cycles of approximately nine years duration. The reactions of the PPII and PPIII branches of the proton-proton chain are producing neutrinos through the  $^7\text{Be}$ - and  $^8\text{B}$ - reactions. If one assumes that a dampening mechanism operates for three reactions of the PPII and PPIII branches as discussed above, the variations of the argon production in the Homestake experiment over time can be explained on purely statistical arguments based on lifetimes and their ratios for the three reactions. For these nuclear reactions, destruction and dampening may work opposite to each other. If the

destruction rate is approximately three times the dampening rate, if the destruction is  $\sqrt{3}b$  for some  $b > 0$ , and if the dampening effect starts  $\frac{3}{4}b$

time units from the starting time  $t = 0$ , then the time variation cycles seen in the argon production in the Homestake experiment can be reproduced by considering a scenario of three sets of reactions of the PPII and PPIII branches of the proton-proton chain, one set with  $b = 1$  unit of time, say 9 years, the second set consisting of 5 successive reactions with  $b = 0.2$  time units each, and the third set consisting of 8 successive reactions with  $b = 0.125$  time units each.

### References

- Abdurashitov, J.N. et al.: 1994, Phys. Lett. B328, 234.
- Anselmann, P. et al.: 1994, Phys. Lett. B327, 377.
- Bahcall, J.N. and Pinsonneault, M.H.: 1992, Rev. Mod. Phys. 64, 885.
- Castellani, V. et al.: 1994, Phys. Rev. D50, 4749.
- Davis Jr., R.: 1993, in Y. Suzuki and K. Nakamura (eds.), 'Frontiers of Neutrino Astrophysics', Universal Academy Press, Inc., Tokyo.
- Haubold, H.J. and Gerth, E.: 1990, Solar Physics 127, 347.
- Haubold, H.J. and Mathai, A.M.: 1994, in H.J. Haubold and L.I. Onuora (eds.), 'Basic Space Science', AIP Conference Proceedings Vol. 320, American Institute of Physics, New York.
- Kiko, J.: 1995, The GALLEX solar neutrino experiment at the GranSasso Underground Laboratory; these Proceedings.
- Mathai, A.M. and Haubold, H.J.: 1988, Modern Problems in Nuclear and Neutrino Astrophysics, Adademie-Verlag, Berlin.
- Mathai, A.M.: 1993, Canad. J. Statist. 21, 277.
- Nakamura, K.: 1993, Nucl. Phys. Suppl. B31, 105.

Table captions:

Table 1: Predictions of the Standard Solar Model for the Kamiokande, Homestake, and GranSasso/Baksan experiments (Bahcall and Pinsonneault, 1992).

Table 2: The four currently operating solar neutrino experiments.

Table 3: Predicted capture rates in SNU from various flux components of the pp-chain and CNO cycle for the Homestake and GranSasso/Baksan experiments. The uncertainties are the total theoretical range,  $\sim 3\sigma$  (Bahcall and Pinsonneault, 1992).

Table 4: Comparison of the detected rates of the four solar neutrino experiments with the predicted rates of the Standard Solar Model (Bahcall and Pinsonneault, 1992). The Kamiokande flux is in units of  $10^6 \nu cm^{-2} s^{-1}$ , while the Homestake and GranSasso/Baksan rates are in SNU.

Table 5: For the destruction-dampening mechanism considered here, the area of the triangle governing reaction 1, the combined areas of the 5 triangles for reaction 2, and the combined areas of the 8 triangles of reaction 3, are proportional to the combination of three sources to the total capture rate of the Homestake experiment.

Figure captions:

- Fig. 1: The proton-proton chain and its three different branches to accomplish to formation of  ${}^4\text{He}$ .
- Fig. 2: The neutrino production as a function of the dimensionless distance variable  $x = R/R_{\odot}$  in the Standard Solar Model of Bahcall and Pinsonneault (1992).
- Fig. 3: The argon-production rate detected by the Homestake experiment from 1970.8 to 1991.6 (Davis, 1993).
- Fig. 4: The five-point moving average of the argon-production rate data as shown in Figure 3.
- Fig. 5: Power spectrum of the argon-production rate data in Figure 3 obtained by Fourier analysis.
- Fig. 6: A non-symmetric Laplacian, slowly rising and rapidly falling. The function  $g(u)$  is the density of  $u$ , describing the destruction-dampening mechanism for nuclear reactions involving species  $i$ .
- Fig. 7: The behaviour of the function  $A$  in (24) denoting the total destruction of species  $i$ .
- Fig. 8: The non-symmetric Laplacian shown in Figure 6 can be approximated by a non-symmetrical triangle.
- Fig. 9: The destruction-dampening mechanism in (25) and (26), where the Laplacians has been approximated by triangles, can reproduce the time variation of the original argon-production rate within the range of the error bars attached to each run.

This figure "fig1-1.png" is available in "png" format from:

<http://arxiv.org/ps/astro-ph/9502075v1>

This figure "fig2-1.png" is available in "png" format from:

<http://arxiv.org/ps/astro-ph/9502075v1>

This figure "fig1-2.png" is available in "png" format from:

<http://arxiv.org/ps/astro-ph/9502075v1>

This figure "fig2-2.png" is available in "png" format from:

<http://arxiv.org/ps/astro-ph/9502075v1>

This figure "fig1-3.png" is available in "png" format from:

<http://arxiv.org/ps/astro-ph/9502075v1>

This figure "fig2-3.png" is available in "png" format from:

<http://arxiv.org/ps/astro-ph/9502075v1>